

Highly and Rapidly Stabilized Protocrystalline Silicon Multilayer Solar Cells

Koeng Su Lim, Joong Hwan Kwak, Seong Won Kwon, and Seung Yeop Myong
Department of Electrical Engineering & Computer Science, KAIST, 373-1 Guseong-dong,
Yuseong-gu, Daejeon 305-701, Republic of Korea

ABSTRACT

We have developed highly stabilized (p-i-n)-type protocrystalline silicon (pc-Si:H) multilayer solar cells. However, the source of the superior light-induced stability of the pc-Si:H multilayer absorbers compared to conventional amorphous silicon (a-Si:H) absorbers remains unclear. Photoluminescence (PL) and Fourier transform infrared (FTIR) spectroscopy measured at room temperature produce strong evidence that nano-sized silicon grains embedded in regularly arranged highly H₂-diluted sublayers suppress the photocreation of dangling bonds. To achieve a high conversion efficiency, we applied a double-layer p-type amorphous silicon-carbon alloy (p-a-Si_{1-x}C_x:H) structure to the pc-Si:H multilayer solar cells. The less pronounced initial short wavelength quantum efficiency variation as a function of bias voltage, and the wide overlap of dark current - voltage (J_D - V) and short-circuit current - open-circuit voltage (J_{sc} - V_{oc}) characteristics prove that the double p-a-Si_{1-x}C_x:H layer structure successfully reduces recombination at the *p/i* interface. Thus, we achieved a highly stabilized efficiency of 9.0 % without any back reflector.

INTRODUCTION

Thin film silicon solar cells employing amorphous silicon (a-Si:H) based absorbers have attracted great interest in the industrial realm due to their easy optical band gap design, low-temperature, low-cost, and large-scale production. However, a-Si:H exhibits serious light-induced degradation called the Staebler-Wronski effect [1]. The H₂ dilution of SiH₄ has attracted great interest in efforts to suppress the Staebler-Wronski effect in a-Si:H based material. Recently, so-called "edge" materials such as single layers of H₂-diluted protocrystalline silicon (pc-Si:H) or nanocrystalline silicon (nc-Si:H) [2-6] were shown to be better absorbers than conventional H₂-diluted a-Si:H due to their higher stability and vertical photosensitivity (the ratio of photo- to dark-conductivity). Because the former is fabricated just below the threshold of an amorphous-to-microcrystalline transition and the latter is fabricated just above the threshold of the transition, such depositions are very sensitive to the film thickness and H₂ dilution.

An a-Si:H/H₂-diluted microcrystalline silicon (μ c-Si:H) superlattice has been proposed as the most promising absorber due to its (i) isotropic transport properties achieved by perturbing the columnar growth of μ c-Si:H [7] and (ii) lower sensitivity to the film thickness and H₂ dilution than single layers of edge materials. However, this structure is unsuitable for mass production because of the discrete deposition of its sublayers. Therefore, we have developed pc-Si:H multilayer absorbers that are prepared by alternate H₂ dilution under continuous ultraviolet (UV) light irradiation using a photoassisted chemical vapor deposition (photo-CVD) system [8-10] as a practical simulation of the previous a-Si:H/ μ c-Si:H superlattice. The pc-Si:H multilayer absorbers have the advantages of excellent light-induced stability and fast annealing behavior. In

this way, highly stabilized thin film solar cells were developed in our previous work [11]. We observed faster stabilization and recovery by thermal annealing of the pc-Si:H multilayer solar cells compared with those of a-Si:H and pc-Si:H single layer solar cells [8,11]. Based on the observed short time constants for light-induced degradation or thermal annealing of the multilayers, Jun *et al.* suggested rapid hydrogen motion in the layered structure, due to the spatial separation of regimes with improved medium range order from regimes where hydrogen is confined [8]. (Specifically the absence of Si-H bonds near weak bonds impedes breaking of these bonds.) The origin of the excellent light-soaking behavior is still being debated, however, because these authors could not provide unequivocal evidence for their expectation. In this paper, we demonstrate a quantum-size-effect (QSE) associated with nc-Si grains regularly distributed in a well-ordered a-Si:H matrix and investigate its impact on the light-soaking behavior of the multilayer.

EXPERIMENTAL

Using a photo-CVD system, we fabricated i-pc-Si:H multilayers and (p-i-n)-type solar cells at 250 °C. To dissociate the reactant gases, we used a low-pressure mercury (Hg) lamp with resonance lines of 184.9 nm and 273.7 nm as a UV light source. For characterization, we deposited the i-pc-Si:H multilayers onto textured SnO₂ coated glass (Asahi U-type glass) and onto c-Si wafers by the Hg-sensitized photo-CVD technique, modulating a mixture of SiH₄ and H₂ gases. We prepared the widely-used undiluted p-a-Si_{1-x}C_x:H window layers of the solar cells by a direct photo-CVD technique with a mixture of Si₂H₆, B₂H₆, and C₂H₄ reactant gases. We prepared a H₂-diluted p-a-Si_{1-x}C_x:H buffer using the Hg-sensitized decomposition of a mixture of SiH₄, H₂, B₂H₆, and C₂H₄ reactant gases based on a previously-reported process for the deposition of H₂-diluted p-a-Si_{1-x}C_x:H that incorporated nc-Si grains [12-15]. This H₂-diluted p-a-Si_{1-x}C_x:H has a higher electrical conductivity, optical transmittivity, carrier mobility, and doping efficiency than undiluted p-a-Si_{1-x}C_x:H.

Raman spectra were measured using a JASCO Corp., NRS-1000 system. The wavelength of the Ar laser is 532 nm. The PL spectra were obtained at room temperature by using a He-Cd laser (typically 40 mW at $\lambda = 325$ nm). We failed to perform electron spin resonance (ESR) measurements of the i-pc-Si:H multilayers because their densities of neutral DBs were lower

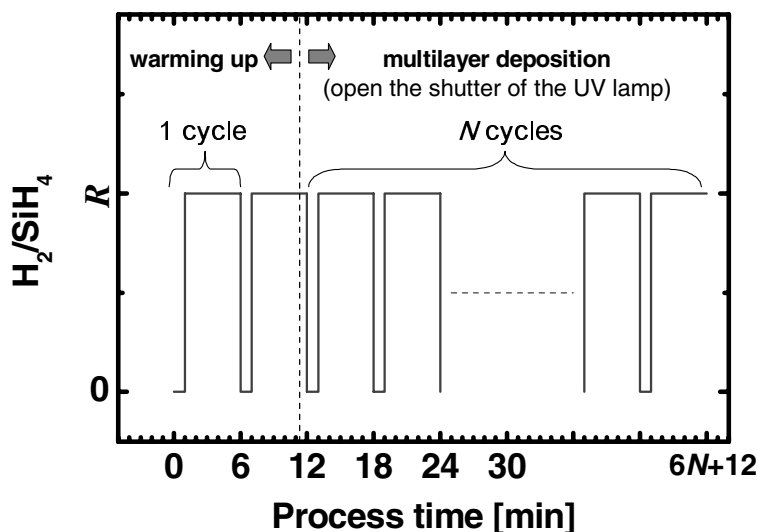


Figure 1. Schematic diagram of the hydrogen dilution (H_2/SiH_4) modulation for an i-pc-Si:H multilayer deposition.

than the detection limit. The cell characteristics were measured under 100 mW/cm^2 (AM 1.5) solar simulator irradiation. We also measured the initial quantum efficiency (QE) of the solar cells in the short wavelength region centered at 400 nm by varying the applied voltage from -1 to 0.4 V with a step increment of 0.2 V . The dark current - voltage (J_D - V) and short-circuit current - open-circuit voltage (J_{sc} - V_{oc}) characteristics were measured at room temperature. The latter was achieved by varying the illumination intensity in the range of 10^{-7} to 1 sun ($J_{sc} = 10^{-9} - 10^{-2} \text{ mA/cm}^2$).

Figure 1 shows a schematic diagram of alternating hydrogen dilution (H_2/SiH_4) for an i-pc-Si:H multilayer preparation performed using the photo-CVD technique. The i-pc-Si:H multilayer consists of low H_2 -dilution and high H_2 -dilution a-Si:H sublayers. This repetitively layered structure is deposited by simply toggling the mass flow control of H_2/SiH_4 between 0 and R under continuous UV light irradiation. Due to the continuous deposition, all interfaces are graded in H-content and the average deposition rate of the multilayer is comparable to that of conventional undiluted i-a-Si:H [11]. During the deposition, however, the chamber pressure was also slightly toggled with the gas flow control because the angle of an automatic pressure controller (APC) was maintained at a constant value. To find an optimal layered structure, we deposited multilayers with R changing from 15 to 30 . We also varied the total number of cycles of H_2/SiH_4 modulation (N) in order to keep the thickness of the multilayers constant at $\sim 550 \text{ nm}$. Thus, we increased N with the increase in R , because the hydrogen exposure near the growing surface increases during both the low H_2 -dilution and high H_2 -dilution a-Si:H sublayer depositions due to the continuous deposition while maintaining a constant angle of the APC.

RESULTS AND DISCUSSIONS

Figure 2 displays Raman spectra of a series of i-pc-Si:H multilayers prepared at different R of the high H_2 -dilution sublayers and a single layer prepared at constant $R = 15$. We note that $\sim 550 \text{ nm}$ thick multilayers fail to show any distinct fraction of the $\mu\text{-Si:H}$ phase, whereas the 300 nm thick single layer indicates a $\mu\text{-Si:H}$ phase. We speculate that $\sim 10 \text{ nm}$ thick low H_2 -dilution sublayers [11] interrupt the columnar growth of $\mu\text{-Si:H}$.

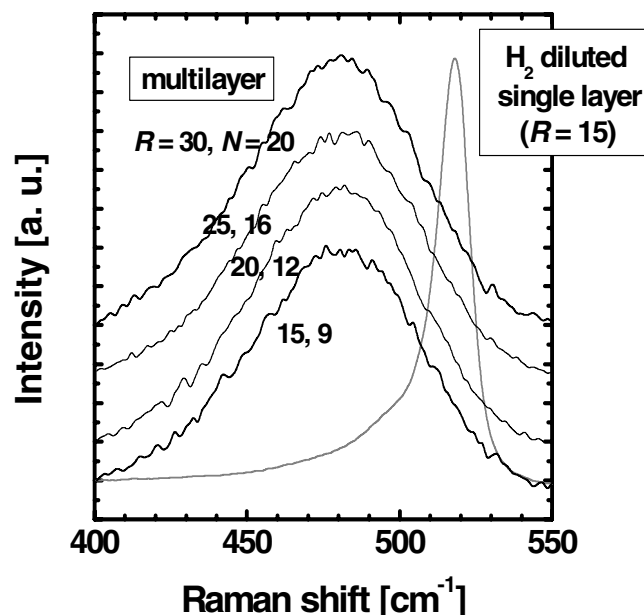


Figure 2. Raman spectra of a series of i-pc-Si:H multilayers prepared at different R for the high H_2 -dilution sublayers and a H_2 -diluted single layer (300 nm) prepared at $R = 15$.

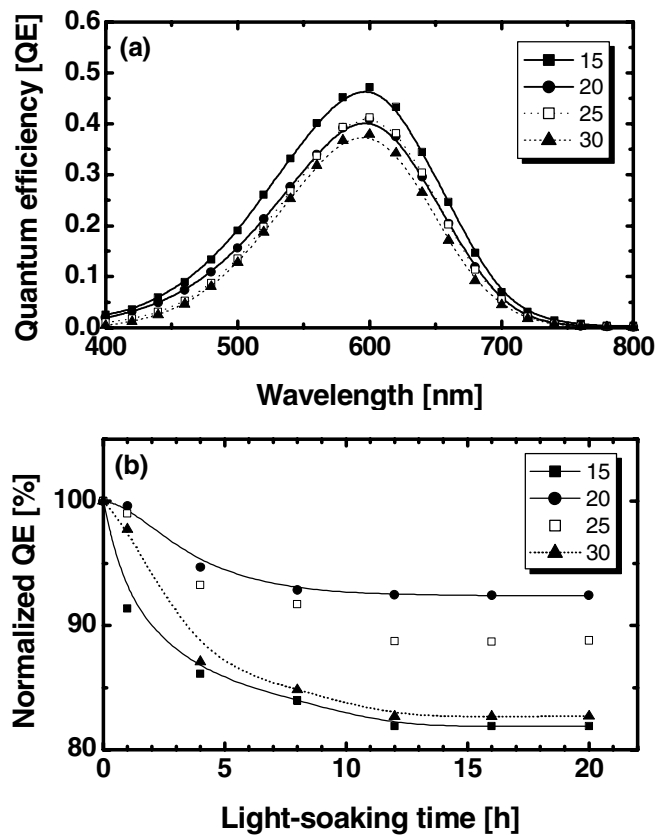


Figure 3. R dependence of the quantum efficiency (QE) of glass/SnO₂/i-pc-Si:H multilayer (~ 550 nm)/Al structures. (a) initial QE (b) light-soaking behavior of normalized QE at the wavelength of 600 nm.

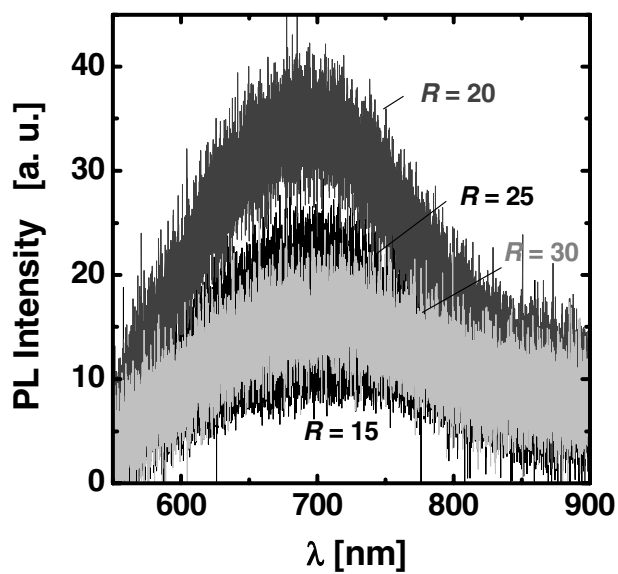


Figure 4. PL spectra of i-pc-Si:H multilayers measured at room temperature.

To investigate the light-induced stability of the multilayers, we fabricated diodes with a structure of glass/SnO₂/i-pc-Si:H multilayer(~550 nm)/Al. Figure 3 shows the R dependence of the initial quantum efficiency (QE). We found in Fig. 3 (a) that the initial QE declines with increasing R . All multilayers show their maximum values of the initial QE at a wavelength (λ) of 600 nm. In Fig. 3 (b) we found that all multilayers exhibit fast light-induced stabilization of the normalized QE at $\lambda = 600$ nm. From these figures, it is found that the optimum R for stable absorbers is 20.

Figure 4 exhibits the photoluminescence (PL) spectra of the multilayers measured at room temperature. All samples show a broad and small peak near 690 nm. Since it is known that both bulk nc-Si:H and a-Si:H films exhibit no visible PL at room temperature, we suggest that the PL of the multilayers arises from the quantum-size-effect (QSE) of the nanocrystallites in the high H₂-dilution sublayers, which are confined by their neighboring low H₂-dilution sublayers along the sample growth direction [16]. This result is supported by the transmission electron microscopy (TEM) studies of Ito *et al.* who have observed ~ 5 nm size spherical nc-Si grains embedded in the i-pc-Si:H multilayers prepared by plasma enhanced chemical vapor deposition (PECVD) [17]. In Fig. 4, it is found that the highest peak PL is obtained for the most stable multilayer. For $R > 20$, the PL spectra show a redshift.

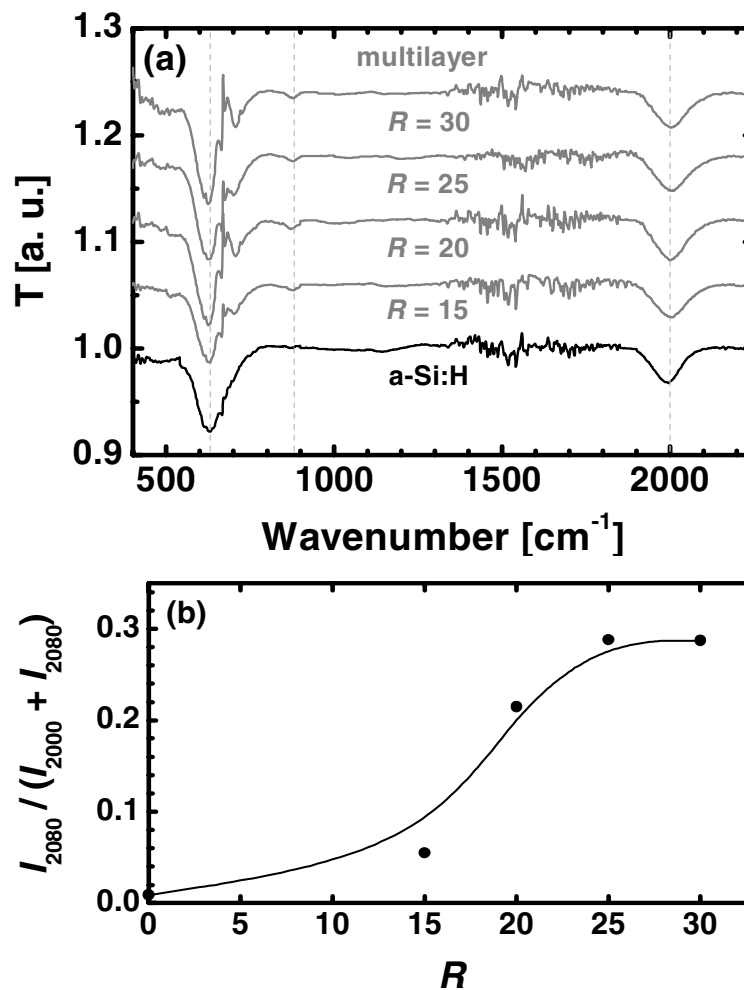


Figure 5. FTIR spectroscopy of an undiluted a-Si:H layer and i-pc-Si:H multilayers: (a) FTIR spectra: (b) microstructure factor. $I_{2080}/(I_{2000}+I_{2080})$. $R=0$ indicates the undiluted a-Si:H.

Figure 5 (a) provides Fourier transform infrared (FTIR) spectra of a single undiluted i-a-Si:H layer and the i-pc-Si:H multilayers prepared on c-Si. The undiluted i-a-Si:H exhibits absorption peaks centered at 630, 880, and 1990 cm^{-1} . With the increase in R of the multilayers, the main Si-H wagging vibrational mode typical of a-Si:H gradually shifts downward to $\sim 612 \text{ cm}^{-1}$, which can be assigned to monohydride (SiH) bonding on c-Si(100) surfaces [18]. Thus, this frequency shift can be attributed to the inclusion of crystallites in the high H_2 -dilution sublayers. In the case of the multilayers, the Si-H stretching vibrational mode of a-Si:H centered at 1990 cm^{-1} shifts upward to 2000 cm^{-1} and new component centered at $\sim 2080 \text{ cm}^{-1}$ emerges. Because we failed to detect any microvoids by small-angle x-ray scattering (SAXS) for our pc-Si:H samples, the latter peak can be attributed to the stretching vibrational mode of dihydride (SiH_2) bonding groups [19] or clustered Si-H bonds in grain boundary regions [20-21]. We assign the $\sim 2080 \text{ cm}^{-1}$ absorption peak of the multilayers to clustered Si-H bonds in grain boundary regions, an assignment supported by the appearance of the peak at $\sim 612 \text{ cm}^{-1}$ [6]. The enlargement of the doublet centered at 880 cm^{-1} , corresponding to the vibrational mode of higher order Si-H, also supports the assignment of the peak at $\sim 2080 \text{ cm}^{-1}$. Thus, the appearance of the $\sim 2080 \text{ cm}^{-1}$ absorption peak as well as the $\sim 612 \text{ cm}^{-1}$ absorption peak can be ascribed to the inclusion of small crystallites in the high H_2 -dilution sublayers. From the spectra, we have evaluated the microstructure factor, $I_{2080}/(I_{2000}+I_{2080})$, where I_i denotes the area under a Gaussian peak centered at position i . In the case of the undiluted a-Si:H, I_{2000} is evaluated from the area under the Gaussian peak centered at 1990 cm^{-1} . In Fig. 5 (b), this factor is shown to increase with increasing R of the multilayers.

We performed a light-soaking test of the multilayer cell via 100 h 1-sun light illumination.

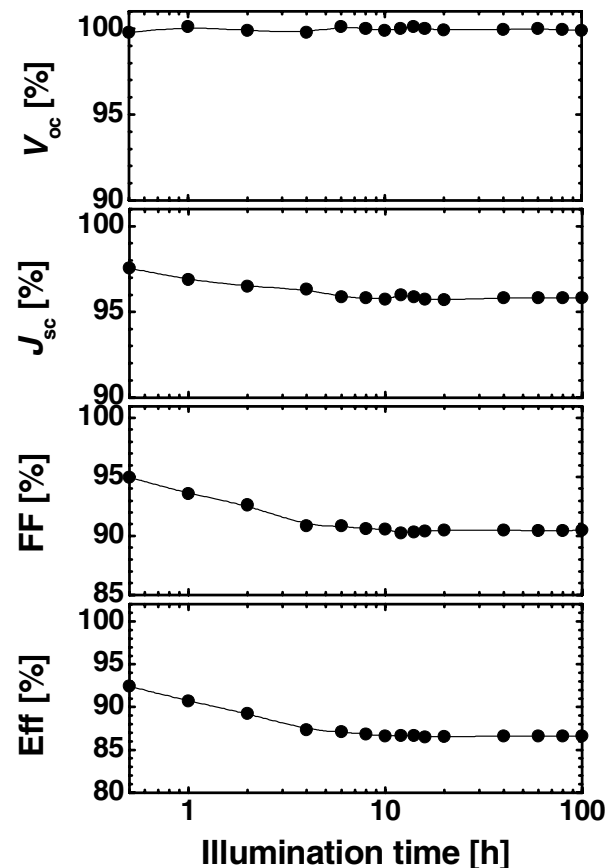


Figure 6. Normalized light-soaking behavior of a pc-Si:H multilayer solar cell.

Figure 6 shows the normalized light-soaking behavior of a (p-i-n)-type pc-Si:H multilayer solar cell with the following structure: glass/SnO₂/undiluted p-a-Si_{1-x}C_x:H/H₂-diluted p-a-Si_{1-x}C_x:H /i-pc-Si:H multilayer (640 nm, $R = 20$)/n- μ c-Si:H/Al (cell area: 0.092 cm²). In order to determine the optical constants of the undiluted p-a-Si_{1-x}C_x:H window layer, we performed spectroscopic ellipsometry (SE) measurements with a phase-modulated spectroscopic ellipsometer (UVISSEL-Jobin Yvon) [22-23]. From the SE analysis, we discovered a natural hydrogen treatment process that involves etching the defective undiluted p-a-Si_{1-x}C_x:H window layer and improving order in the window layer. This effect occurs in the initial stage when the highly conductive, low absorption, and well-ordered H₂-diluted buffer layer is deposited onto the window layer [11, 24-25]. Due to this natural hydrogen treatment effect, we can effectively reduce the recombination at the p/i interface, resulting in a dramatic improvement of all solar cell parameters including V_{oc} , J_{sc} , and fill factor (FF) [11]. Consequently, we have achieved a considerable initial conversion efficiency of 10.4 % ($V_{oc} = 0.920$ V, $J_{sc} = 15.6$ mA/cm², and FF = 0.721) without any back reflector. If we do not use the H₂-diluted p-a-Si_{1-x}C_x:H buffer layer, the initial efficiency is reduced significantly to 7.7 % due to the decrease in all parameters ($V_{oc} = 0.845$ V, $J_{sc} = 13.6$ mA/cm², and FF = 0.670). The extent of the improvement for the multilayer cell is smaller than that for a-Si:H solar cells [24-25]. Since the first layer of the i-pc-Si:H multilayer is an ultrathin (~ 5 nm) high H₂ dilution sublayer, the multilayer cell without the H₂-diluted p-a-Si_{1-x}C_x:H buffer also involves a weak natural hydrogen treatment during the p/i interface formation. Therefore, the improvement of the multilayer cell by the natural treatment effect during the formation of the double p-a-Si_{1-x}C_x:H layer structure diminishes.

For the pc-Si:H multilayer solar cell, we have achieved a stabilized efficiency of 9.0 % ($V_{oc} = 0.919$ V, $J_{sc} = 15.0$ mA/cm², FF = 0.652, and degradation ratio = 13.4 %) after 12 h 1-sun (100 mW/cm², AM 1.5) light irradiation. Due to its stable V_{oc} , the pc-Si:H multilayer solar cell exhibits weak degradation behavior. Thus, the H₂-diluted p-a-Si_{1-x}C_x:H buffer layer contributes to the improvement of the stabilized efficiency by enhancing V_{oc} . The FF exhibits the largest light-induced degradation effect. Furthermore, the stabilized multilayer cell displays a perfect

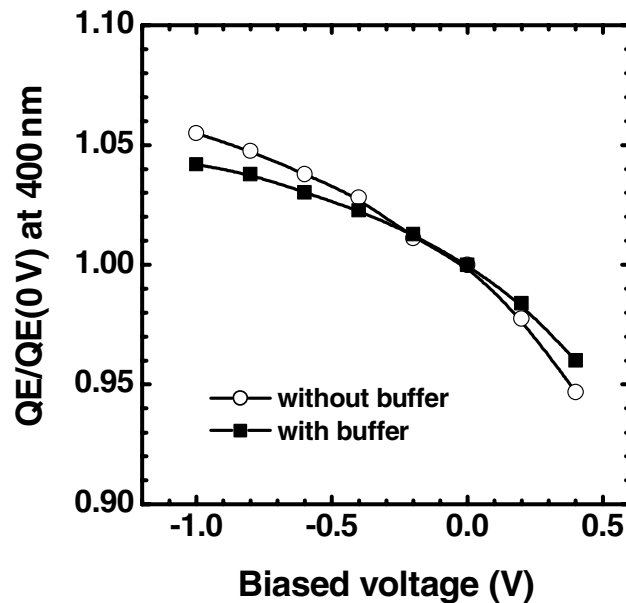


Figure 7. Ratios of QE (V) to QE (0 V) at the short wavelength of 400 nm. These values are evaluated from the initial QE of the pc-Si:H multilayer solar cell.

recovery to its initial value after 1 h thermal annealing at 133 °C, whereas an a-Si:H solar cell with the same structure shows a recovery of 94 %. Thus, the pc-Si:H multilayer solar cell has faster annealing behavior than a-Si:H solar cells.

Figure 7 depicts the dependence of the QE (at the wavelength of 400 nm) on bias voltage. The optimized multilayer cell with the H₂-diluted p-a-Si_{1-x}C_x:H buffer layer exhibits less variation at the short wavelength than its bufferless analog. This can be attributed to a higher electric field and well-ordered structure formed by applying the H₂-diluted p-a-Si_{1-x}C_x:H layer at the p/i interface. We conclude that the lightly-doped H₂-diluted p-a-Si_{1-x}C_x:H buffer layer successfully reduces the recombination at the heterojunction interface by blocking diffusion of boron into the i-pc-Si:H and by relaxing the strain [26]. Compared to a-Si:H cells [20-21], the bufferless multilayer cell shows a smaller variation at 400 nm. This can be ascribed to the aforementioned weak natural hydrogen treatment effect during the p/i interface formation in the latter cell.

The J_D - V characteristics of the pc-Si:H multilayer cells can be investigated to inspect the contribution of the p/i interface to V_{oc} . J_D of the multilayer cells can be expressed as

$$J_D = J_o [\exp(qV/nkT)-1], \quad (1)$$

where J_o is the reverse saturation current density, n is the diode quality factor, q is the electric charge, k is Boltzmann's constant, and T is the absolute temperature. The effect of the p/i interface on V_{oc} can be identified from its dependence on the light illumination intensity. Applying a simplified model in which series and shunt resistance effects are negligible and the photocurrent density has no voltage dependence, we obtain

$$J_{sc} = J_o [\exp(qV_{oc}/nkT)-1], \quad (2)$$

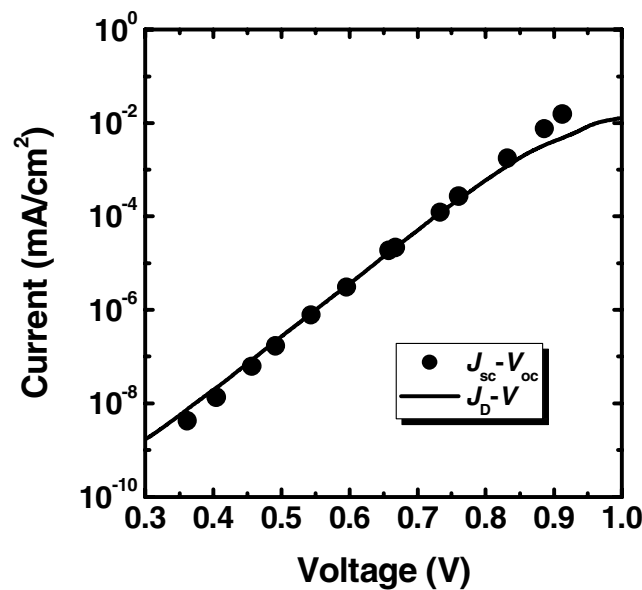


Figure 8. Initial J_D - V characteristics of the pc-Si:H multilayer solar cell superimposed on its J_{sc} - V_{oc} characteristics.

by substituting J_{sc} and V_{oc} for J_D and V in Eq. (1), respectively.

The initial J_D - V and J_{sc} - V_{oc} characteristics of the pc-Si:H multilayer cell are shown in Fig. 8. Due to the reversible recovery of the multilayer cell by thermal annealing, its initial characteristics are the same as those in the annealed state. For $V < 0.74$ V, J_D shows an exponential dependence on V . In this regime, the carrier transport with $n = 1.53$ can be ascribed to the injection of electrons and holes from the n- μ c-Si:H layer and the p-a-Si_{1-x}C_x:H layers, respectively, which is followed by their diffusion and ultimate recombination [27]. For $V \geq 0.74$ V, J_D is limited by series resistance [28] and by a transition from diffusive to drift transport [29]. We should note that the J_D - V characteristics with $n = 1.45$ agree well with the bulk recombination dominant J_{sc} - V_{oc} characteristics except for $V_{oc} \geq 0.8$ V. The wide overlap means that our multilayer cell is free from recombination at the p/i interface [30] by the natural hydrogen treatment effect during the formation of the double p-a-Si_{1-x}C_x:H layer structure.

Figure 9 exhibits the band diagram that explains the improvement of the built-in potential (ΔV_{bi}) by using the highly conductive H₂-diluted p-a-Si_{1-x}C_x:H buffer layer, which can be expressed as [22]

$$\Delta V_{bi} = \Delta\phi_b + \Delta E_{va}. \quad (3)$$

It is believed that the high conductivity of the buffer layer improves the built-in potential of a-Si:H solar cell by: (i) lowering the potential barrier ($\Delta\phi_b$) at the SnO₂:F/undiluted p-a-Si_{1-x}C_x:H window layer interface due to the increase in the dark conductivity of the window layer, and (ii) raising the conduction band edge due to a buffer-layer Fermi level location closer to the valence band edge (ΔE_{va}) of the i-pc-Si:H absorber. Due to the improvement of V_{bi} , the cell with the buffer shows a higher V_{oc} than its bufferless analog. This improvement of V_{bi} is also beneficial to prevent electron back diffusion.

Next, we will discuss the origin of the excellent light-induced stability and thermal annealing behavior. Figure 9 also shows the proposed structure of the i-pc-Si:H multilayers including the non-uniform distribution of hydrogen atoms [18] based on the analysis of PL and

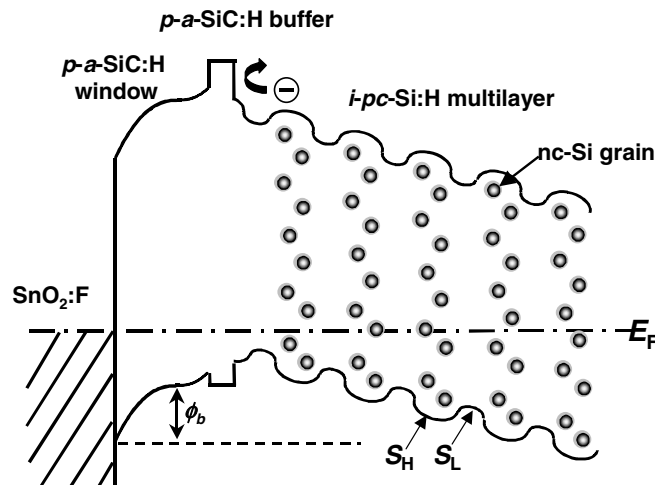


Figure 9. Band diagram of a pc-Si:H multilayer solar cell. S_H and S_L stand for a high H₂-dilution sublayer and a low H₂-dilution sublayer, respectively. ϕ_b denotes the barrier height for holes at the SnO₂:F/undiluted p-a-SiC:H window interface.

FTIR spectroscopy. The multilayer consists of low H_2 -dilution and high H_2 -dilution sublayers. Isolated spherical nc-Si grains are embedded in a well-ordered a-Si:H matrix of high H_2 -dilution sublayers. An a-Si:H grain boundary layer with a high hydrogen concentration surrounds each nc-Si:H grain [31]. This grain boundary layer is the most defective layer in the multilayer. Low H_2 -diluted sublayers which hinder the percolation path of μc -Si:H possess a less-ordered a-Si:H matrix than that of high H_2 -dilution sublayers. All interfaces are graded by H_2 .

We believe that a significant fraction of photoexcited carriers generated in the a-Si:H matrix of both sublayers can diffuse to the grain boundary regions surrounding the nc-Si grains. Because the isolated nc-Si grains have a much larger capture radius (d) than that of the dangling bond (DB) defects ($d \cong$ several Å) [32-33], the isolated nc-Si grains capture the photoexcited carriers. In other words, the isolated nc-Si grains embedded in the high H_2 -dilution sublayers tend to act as radiative recombination centers for photoexcited carriers, and hence suppress the photocreation of DBs due to nonradiative recombination in the a-Si:H matrix. This suggestion is reasonable because the nc-Si grains with a few nanometer size are expected to have a smaller optical band gap than a-Si:H [34]. In the multilayer, the isolated nc-Si grains have a regular distribution due to the spatially regular arrangement of the high H_2 -dilution sublayers. In contrast, the distribution of nc-Si grains is restricted to the near surface in the case of the i-pc-Si:H single layer. Since the recombination in the nc-Si grains is elevated by their uniform distribution and density, the pc-Si:H multilayer solar cells have the faster and higher light-induced stability than a-Si:H and pc-Si:H single layer solar cells (see Ref. 8).

With increasing R of the high H_2 -dilution sublayers, both the thickness of the low H_2 -dilution and high H_2 -dilution sublayers are reduced due to the retardation of growth rate by enhanced hydrogen exposure near the growing surface. Thereby we must increase N in order to maintain the total thickness at ~ 550 nm. We conclude from the redshift of the PL spectra (see Fig. 4) that the average size of the nc-Si:H grains increases with the increase in R . According to the FTIR spectra (see Fig. 5 (a)), we also conclude that the total number of nc-Si grains increases with the increase in R due to the increase in the number of high H_2 -dilution sublayers. Thus the initial photogenerated current decreases due to enhanced recombination in the isolated nc-Si grains (see Fig. 3(a)). The multilayer prepared with $R = 15$ has the thickest and most defective a-Si:H matrix in the low H_2 -dilution sublayers due to the lowest remaining H_2 gas concentration in the reaction chamber during their deposition. In addition, the nc-Si grains with the lowest density and smallest size are formed within the high H_2 -dilution sublayers. Thus, this multilayer shows the highest degradation ratio due to the increased photocreation of DBs in a-Si:H matrix. Compared to this multilayer, the one prepared with $R = 20$ shows a remarkable suppression of DB photocreation. This can be attributed to the improved a-Si:H matrix in both types of sublayers with increased hydrogen dilution, the increased density and grain size of nc-Si, and the reduced thickness of the low H_2 -dilution sublayers. For $R > 20$, the degradation ratio increases again. The volume fraction of the defective a-Si:H grain boundary layers surrounding the nc-Si grains increases with the increase in R . Because the increased nonradiative recombination within the defective grain boundary layers disturbs the radiative recombination in the nc-Si grains, the photocreation of DBs is enhanced in this regime.

The fast recovery by thermal annealing of the pc-Si:H multilayer solar cells compared with that of a-Si:H and pc-Si:H solar cells is mainly due to the low light-induced degradation and non-uniform distribution of hydrogen. (The hydrogen content is highly confined near the nc-Si grains.) The first ultrathin (~ 5 nm) high H_2 -dilution sublayer in the multilayer promotes

perfect recovery by preventing the H^+ drift into the p layer.

Finally, we would like to emphasize that we can describe very well the observed behavior of light-soaked conductivity, SE, and FTIR spectroscopy of i-pc-Si:H single layers as a function of hydrogen dilution ratio as reported in Ref. 5 by using the demonstrated role of isolated nc-Si grains in the a-Si:H matrix and defective grain boundary layers surrounding these grains.

CONCLUSIONS

In summary, we have successfully achieved a highly stable conversion efficiency of 9.0 % for a (p-i-n)-type pc-Si:H multilayer solar cell fabricated by incorporating a double p-a-Si_{1-x}C_x:H structure and an i-layer with a multilayered structure obtained through alternating H₂ dilution. The pc-Si:H multilayer leads to weak light-induced degradation that is superior to conventional a-Si:H and pc-Si:H single layer solar cells due to its rapid stabilization and recovery. Photoluminescence and Fourier transform infrared spectroscopy measured at room temperature produce strong evidence that nc-Si grains embedded in regularly arranged high H₂-dilution sublayers suppress the photocreation of dangling bonds. Fast light-induced stabilization and recovery by thermal annealing are mainly due to the fast recombination in the isolated nc-Si grains embedded within the regularly arranged high H₂-dilution sublayers. Research on the application of back reflectors such as ZnO:H [35] and ZnO:H/Ag is currently attempting to overcome the poor spectral response of the solar cells in the long-wavelength region [11].

ACKNOWLEDGEMENT

The authors gratefully acknowledge the Asahi Glass Company for providing us with Asahi U-type glass substrates.

REFERENCES

1. D. L. Staebler and C. R. Wronski, *Appl. Phys. Lett.* **31**, 292 (1997).
2. J. Koh, Y. Lee, H. Fujiwara, C. R. Wronski and R.W. Collins, *Appl. Phys. Lett.* **73**, 1526 (1998).
3. J. Yang, K. Lord and S. Guha, *Mater. Res. Soc. Symp. Proc.* **609**, A15.4 (2000).
4. C. Koch, M. Ito, V. Švrček, M. B. Schubert and J. H. Werner, *Mater. Res. Soc. Symp. Proc.* **609**, A15.6 (2000).
5. J. Y. Ahn, K. H. Jun, M. Konagai and K. S. Lim, *Appl. Phys. Lett.* **82**, 1718 (2003).
6. Y. Xu, X. Liao, G. Kong, X. Zeng, Z. Hu, H. Diao and S. Zhang, *Technical Digest of The 14th International Photovoltaic Science and Engineering Conference*, Bangkok, Thailand, p. 105 (2004).
7. J. Kočka, J. Stuchlík, Ha. Stuchlíková, V. Švrček, P. Fojtík, T. Mates, K. Luterová and A. Fejfar, *Appl. Phys. Lett.* **79**, 2540 (2001).
8. K. H. Jun, J. D. Ouwers, R. E. I. Schropp, J. Y. Lee, J. H. Choi, H. S. Lee and K. S. Lim, *J. Appl. Phys.* **88**, 4881 (2000).
9. K. S. Lim, S. W. Kwon and S. Y. Myong, *Technical Digest of The 12th International Photovoltaic Science and Engineering Conference*, Jeju, Korea, p. 37 (2001).
10. S. W. Kwon, J. Y. Ahn, S. Y. Myong and K. S. Lim, *Proceedings of the 17th European*

- Photovoltaic Solar Energy Conference and Exhibition*, Munich, Germany, p. 3015 (2001).
11. S. Y. Myong, S. W. Kwon, M. Konagai and K. S. Lim, *Sol. Energy Mater. Sol. Cells* **85**, 133 (2005).
 12. S. Y. Myong, H. K. Lee, E. Yoon and K. S. Lim, *J. Non-Cryst. Solids* **298**, 131 (2002).
 13. H. K. Lee, S. Y. Myong, K. S. Lim and E. Yoon, *J. Non-Cryst. Solids* **316**, 297 (2003).
 14. S. Y. Myong, T. H. Kim, K. H. Kim, B. T. Ahn, S. Miyajima, M. Konagai and K. S. Lim, *Sol. Energy Mater. Sol. Cells* **81**, 485 (2004).
 15. S. Y. Myong, O. Shevaleevskiy, S. Miyajima, M. Konagai and K. S. Lim, *J. Non-Cryst. Solids* **351**, 89 (2005).
 16. S. Tang, X. Liu and X. Bao, *Appl. Phys. Lett.* **66**, 469 (1995).
 17. M. Ito, M. Kondo and A. Matsuda, *Technical Digest of The 14th International Photovoltaic Science and Engineering Conference*, Bangkok, Thailand, p. 381 (2004).
 18. A. H. Mahan, J. Yang, S. Guha and D. L. Williamson, *Phys. Rev. B* **61**, 1677 (2000).
 19. G. Ambrosone, U. Coscia, S. Lettieri, P. Maddalena and C. Minarini, *Materials Science and Engineering B* **101**, 236 (2003).
 20. T. Itoh, K. Yamamoto, K. Ushikoshi, S. Nonomura and S. Nitta, *J. Non-Cryst. Solids* **266**, 201 (2000).
 21. D. Han, K. Wang, J. M. Owens, L. Gedvilas, B. Nelson, H. Habuchi and M. Tanaka, *J. Appl. Phys.* **93**, 3776 (2003).
 22. S. Y. Myong, S. S. Kim and K. S. Lim, *Thin Solid Films* **455**, 482 (2004).
 23. S. Y. Myong, S. S. Kim and K. S. Lim, *Appl. Phys. Lett.* **84**, 5416 (2004).
 24. S. Y. Myong, S. S. Kim and K. S. Lim, *J. Appl. Phys.* **95**, 1525 (2004).
 25. S. Y. Myong and K. S. Lim, *Appl. Phys. Lett.* **86**, 033506 (2005).
 26. R. R. Arya, A. Catalano and R. S. Oswald, *Appl. Phys. Lett.* **49**, 1089 (1986).
 27. J. Deng, J. M. Pearce, R. J. Koval, V. Vlahos, R. W. Collins and C. R. Wronski, *Appl. Phys. Lett.* **82**, 3023 (2003).
 28. H. Sakai, T. Yoshida, S. Fujikake, T. Hama and Y. Ichikawa, *J. Appl. Phys.* **67**, 3494 (1990).
 29. K. Lips, *Mater. Res. Soc. Symp. Proc.* **377**, 455 (1995).
 30. J. M. Pearce, R. J. Koval, A. S. Ferlauto, R. W. Collins, C. R. Wronski, J. Yang and S. Guha, *Appl. Phys. Lett.* **77**, 3093 (2000).
 31. Y. Lubianiker, J. D. Cohen, H. C. Jin and J. R. Abelson, *Phys. Rev. B* **60**, 4434 (1999).
 32. T. Kamei, P. Stradins and A. Matsuda, *Appl. Phys. Lett.* **74**, 1707 (1999).
 33. R. A. Street, "Hydrogenated Amorphous Silicon", ed. R. W. Cahn, E. A. Davis and I. M. Ward (Cambridge University Press, Cambridge, 1991).
 34. T. Shimizu, *Jpn. J. Appl. Phys.* **43**, 3257 (2004).
 35. S. Y. Myong and K. S. Lim, *Appl. Phys. Lett.* **82**, 3026 (2003)